Quantum Monte Carlo study of pressure melting in Yukawa systems

Y. Joanna Wong* and G. V. Chester
Laboratory of Atomic and Solid State Physics, Cornell University, Ithaca, New York 14853-2501
(Received 16 November 1987)

The phase diagram of the Yukawa system at finite temperatures is explored by quantum Monte Carlo simulations. The path-integral method uses the primitive approximation for the density matrix of distinguishable particles; exchange effects are not included in our simulations. Previous zero-temperature calculations have found that both ground-state Yukawa fermions and bosons have two melting transitions. As the density increases, the stable phase changes from the low-density fluid phase to the solid phase and then to a high-density fluid phase. The melting transition at high density is referred to as pressure melting. In our work, the solid-fluid transition is estimated from the stability of the initial lattice during a Monte Carlo run. Our quantum simulations have successfully demonstrated pressure melting at finite temperatures in systems with de Boer parameters $\Lambda^*=0.004$ and 0.005. This results from the soft-core interaction in the quantum systems and is not seen in our classical Yukawa simulations. No solid is found at $\Lambda^*=0.01$. Since previous studies show that there is no ground-state Yukawa solid when the system is sufficiently quantum mechanical, our work suggests that there is no quantum Yukawa solid with $\Lambda^*=0.01$ at any temperature and any density.

I. INTRODUCTION

The phase diagram of superdense Coulombic matter has been a subject of longstanding interest. Studies have been mainly confined to either the charged Coulombic matter or the repulsive Yukawa potential[1-7] (the screened Coulomb potential). Kirzhnits[8] suggested a closed loop for the solid-fluid coexistence of positive nuclei in a homogeneous background of electron gas. Each nucleus in the solid was approximated by an oscillator confined in the potential well defined by its neighbors. Both kinetic and potential energies increase with increasing density, but for the soft-core systems, the kinetic energy increases more rapidly than the potential energy. Many authors have suggested that the solid will be unstable when these energies are of the same order of magnitude. The upper melting transition at high density, where the pressure is high, is referred to as pressure melting and does not exist for classical systems. The phase diagrams of both the charged Bose and Fermi gases in a uniform neutralizing background have been discussed by several authors.[2,4,5,9] Glyde *et al.*[10] have obtained the variational upper bounds for the ground-state energies of the fluid phases for bosons and fermions. There are also exact Monte Carlo calculations for the ground-state energies of both the Bose and Fermi one-component plasma by Ceperley and Alder.[11,12] Hansen, Jancovici, and Schiff[2] used quasiharmonic theory to interpolate the coexistence curve between the classical and quantum regimes. They did this by assuming that Lindemann law of melting holds at all temperatures. Mochkovitch and Hansen[5] later modified this approach and used a generalized Lindemann ratio at melting, which included the changes due to the quantum nature of the system. The Lindemann ratios at melting for ground-state bosons and fermions are very different from the classical ratio. The phase diagrams they obtained for both the charged Bose and Fermi one-component plasma have maximum melting temperatures and bounded solid phases. However, there has not been any direct exploration of the phase diagram of the one-component plasma at finite temperatures where quantum effects are important.

Since it is the soft interaction at short range which produces the high-density pressure melting of the one-component plasma, we expect that pressure melting will also occur in the Yukawa system. The repulsive Yukawa potential has been used to model the Bethe "homework potential" for neutron matter.[3] Ceperley, Chester, and Kalos[13] have performed variational and exact Monte Carlo calculations of the ground-state energy for Yukawa bosons. For the Yukawa fermions,[14] they have obtained variational upper bounds for the ground-state energies. At zero temperature, the free energy is equal to the total energy, and this can be estimated directly from Monte Carlo simulations. The relative stability of the solid and fluid phases at zero temperature can thus be obtained directly by comparing the ground-state energies. As the density is increased from zero, the solid phase eventually becomes more stable than the fluid phase. However, when the solid is compressed to much higher density, the solid will undergo a second phase transition and will melt to the more stable fluid. When the quantum nature becomes sufficiently important, the fluid phase of the Yukawa system always has a lower free energy than the solid. Thus, these Yukawa systems may have no ground-state solid phase at any density. Kawamura[7] has used a quantized lattice-gas model[15,16] to study the solid-fluid transition of the repulsive Yukawa potential. Pressure melting is found for both fermions and bosons, though the phase diagrams are qualitatively different.

The Yukawa potential behaves like the Coulomb potential at short distances, but does not possess the long-

range interaction. In classical simulations of the one-component plasma, the Ewald technique,[17,18] which is commonly used in the potential-energy calculation, is a time-consuming procedure. The Yukawa system has the advantage that it is not necessary to evaluate Ewald sums. In simulations, the spherically symmetric short-range potential is usually truncated at some distances less than half the side of the box which encloses the system. However, the effects of the truncation at the high densities and low temperatures studied need careful examination: we found that the high-density fluid-solid transition is very sensitive to the truncation of the potential. The extended Yukawa potential defined in Sec. II B overcomes this truncation difficulty. Using this potential, we have explored pressure melting at finite temperatures using quantum Monte Carlo simulations based on the path-integral method.[19–23]

To establish the phase diagram rigorously, one must compare the free energies of the solid and fluid phases to determine the thermodynamically stable phase. In our work, we did not calculate free energies but instead have used the stability of the lattice to obtain reasonable estimates of the melting transitions. Our exploratory study used Boltzmann statistics and exchange has not been considered. Exchange effects are insignificant as long as the interparticle spacing is much larger than the de Broglie thermal wavelength or the particles are well localized. This condition is satisfied at most temperatures and densities studied, but we will see from Sec. III B that this assumption no longer holds in the high-density phases we have studied. The results at zero temperature[13,14] lead us to believe that the qualitative phase diagram obtained for the Boltzmann system will not be changed, but the exact melting transition will be sensitive to the statistics of the particles when exchange effects are important. The purpose of this work is to demonstrate pressure melting at finite temperatures in the soft-core Yukawa systems. Since our work is qualitative and exploratory, we did not attempt to locate the solid-fluid transition using free-energy calculations. In our opinion, it will be more appropriate to determine the phase diagram for the repulsive Yukawa system using free-energy calculations when exchange effects are included. We will comment on such calculations at the end of the paper.

The detailed presentation of our work is organized into two sections in this paper—the formalism and the results. Section II A develops the formalism of the path-integral method, using the primitive approximation for the high-temperature density matrix. Section II B gives the details of the model system studied. The results of the simulations are given in Sec. III. Section III A presents the results from both quantum and classical simulations which lead to the schematic phase diagram given in Fig. 9. Section III B compares the thermodynamic properties of the quantum and classical Yukawa systems. We end with some brief comments and discussions of future directions.

II. METHODOLGY

A. Path-integral Monte Carlo simulation

The path-integral Monte Carlo method is based on the discretization of Feynman's path-integral[24,25] formulation of the canonical density matrix. Recently it has been successfully implemented for finite temperature studies of quantum systems.[26–35] Various derivations of the formulation can be found in the literature.[19,22,23,36,37] In statistical mechanics, all thermodynamic quantities of a many-particle system in equilibrium are given by ensemble averages computed with the canonical density matrix, $\rho(\vec{\mathbf{R}},\vec{\mathbf{R}}';\beta)$.[38,39] In classical Monte Carlo simulations, the Metropolis[40] algorithm generates configurations with probability asymptotically given by the Gibbs distribution. The goal in quantum Monte Carlo simulations[41] is to implement algorithms which will sample configurations with probability given by the density matrix. Our formulation of the path-integral method essentially follows that given by Takahashi and Imada.[22]

In simulations, bulk properties of matter are usually studied with a system of N particles in a box with periodic boundary conditions. In coordinate representation, the density matrix for a distinguishable-particle system at temperature T is

$$\rho(\vec{\mathbf{R}},\vec{\mathbf{R}}';\beta)=\langle \vec{\mathbf{R}} \mid \exp(-\beta \mathbf{H}) \mid \vec{\mathbf{R}}' \rangle \ , \tag{1}$$

where $\vec{\mathbf{R}}\equiv(\vec{\mathbf{r}}_1,\vec{\mathbf{r}}_2,\ldots,\vec{\mathbf{r}}_N)$ is the set of $3N$ coordinates of the particles in the system, $\beta=1/k_BT$ is the inverse temperature, $\mathbf{H}=\hat{\mathbf{T}}+\hat{\mathbf{V}}$ is the Hamiltonian,

$$\hat{\mathbf{T}}=-(\hbar^2/2m)\sum_{j=1}^{N}\vec{\nabla}_j^2$$

is the kinetic energy operator of N particles with mass m, and

$$\hat{\mathbf{V}}=\sum_{i=1}^{N-1}\sum_{j=i+1}^{N}v(r_{ij})$$

is the potential energy operator for pairwise interaction $v(r)$ between the particles ($r_{ij}\equiv|\vec{\mathbf{r}}_i-\vec{\mathbf{r}}_j|$ is the distance between the ith and jth particles). Using the closure relation, the density matrix can be rewritten as an integral [within an $(M-1)\times 3N$-dimensional box]

$$\rho(\vec{\mathbf{R}},\vec{\mathbf{R}}';\beta)=\int d\vec{\mathbf{R}}_2\int d\vec{\mathbf{R}}_3\cdots\int d\vec{\mathbf{R}}_M\,\rho(\vec{\mathbf{R}},\vec{\mathbf{R}}_2;\beta/M)\rho(\vec{\mathbf{R}}_2,\vec{\mathbf{R}}_3;\beta/M)\cdots\rho(\vec{\mathbf{R}}_M,\vec{\mathbf{R}}';\beta/M) \ . \tag{2}$$

Each term in the integrand is the N-particle density matrix at a temperature higher than T by a factor M. For sufficiently large M, various acceptable approximations to the high-temperature many-particle density matrix at MT have been presented in the literature.[22,23] With these approximations, the quantum partition function Z_N, which is the trace of the density matrix, is then rewritten as an $(M\times 3N)$-dimensional integral. This can be evaluated by the

Metropolis algorithm as in classical Monte Carlo simulations.

In this work we use what is commonly referred to as the "short-time," or primitive approximation;[19–22,42,43] this is the most straightforward approximation to the many-particle density matrix. The high-temperature density matrix in (2) is obtained by using the lowest-order Trotter formula[44] which gives

$$\exp\left[-\frac{\beta}{M}(\hat{\mathbf{T}}+\hat{\mathbf{V}})\right]=\exp\left[-\frac{\beta}{2M}\hat{\mathbf{V}}\right]\exp\left[-\frac{\beta}{M}\hat{\mathbf{T}}\right]\exp\left[-\frac{\beta}{2M}\hat{\mathbf{V}}\right]+O((\beta/M)^3)\ . \tag{3}$$

The quantum partition function for a N-distinguishable particle system in a three-dimensional cube of side L with periodic boundary conditions is then approximately given by

$$Z_N(\beta)\approx\int\cdots\int_{\text{box}}\prod_{l=1}^{M}\left[d\vec{\mathbf{R}}_l\left[\frac{Mm}{2\pi\beta\hbar^2}\right]^{3N/2}\sum_{\vec{\mathcal{N}}}\exp\left[-\frac{Mm}{2\beta\hbar^2}(\vec{\mathbf{R}}_l-\vec{\mathbf{R}}_{l+1}-L\vec{\mathcal{N}})^2\right]\exp\left[-\frac{\beta}{M}V(\vec{\mathbf{R}}_l)\right]\right], \tag{4}$$

where $\vec{\mathcal{N}}$ is the set of $3N$ discrete integers, and $\vec{\mathbf{R}}_{M+1}\equiv\vec{\mathbf{R}}_1$. The detailed derivations have been outlined in Ref. 22. In our simulations, with the choice M and L used, terms with nonzero vector $\vec{\mathcal{N}}$ make very small contributions to the sum in (4) and so we have included only the $\vec{\mathcal{N}}=\vec{0}$ term in our approximation. Equation (4) then reduces to

$$Z_N(\beta)\approx\int\cdots\int_{\text{box}}\prod_{l=1}^{M}\left[d\vec{\mathbf{R}}_l\left[\frac{Mm}{2\pi\beta\hbar^2}\right]^{3N/2}\exp\left[-\frac{Mm}{2\beta\hbar^2}(\vec{\mathbf{R}}_1-\vec{\mathbf{R}}_{l+1})^2-\frac{\beta}{M}V(\vec{\mathbf{R}}_l)\right]\right], \tag{5}$$

which is the same as that for an infinite system. The periodic boundary conditions, as expected, have a negligible effect on the many-particle density matrix of a sufficiently large system.

From the above discussion, we see that the temperature T plays the role of imaginary time in the formulation of Feynman's path integral; M is often referred to as the number of time slices. Chandler and Wolynes[20,45] have presented an intuitive picture of a classical isomorphism between the quantum partition function given by (5) and that of a polyatomic fluid. The quantum problem of N distinguishable particles is mapped onto a classical problem of N polymer chains with M particles on each chain. The interaction consists of the reduced interpolymer interaction $v(r)/M$, between particles of two different chains with same time index, and the intrapolymer springlike interaction between particles on the same chain with adjacent time indices. Noting that the spring constant $Mm/2\beta^2\hbar^2$ increases with temperature and M, this is suggestive of the decrease in zero-point motion of the particles with increasing temperature. The expression for other thermodynamic quantities, such as potential energy U and pressure P, can be derived by straightforward differentiation of the quantum partition function Z_N. In the primitive approximation, these expressions[22] are similar to those of a classical system of $N\times M$ particles except that the ensemble averages are now weighted by $W(\vec{\mathbf{R}}_1,\ldots,\vec{\mathbf{R}}_M;\beta)$, where

$$W(\vec{\mathbf{R}}_1,\ldots,\vec{\mathbf{R}}_M;\beta)=\left[\frac{Mm}{2\pi\beta\hbar^2}\right]^{3MN/2}\exp\left[-\sum_{l=1}^{M}\frac{Mm}{2\beta\hbar^2}(\vec{\mathbf{R}}_l-\vec{\mathbf{R}}_{l+1})^2-\frac{\beta}{M}\sum_{l=1}^{M}V(\vec{\mathbf{R}}_l)\right]. \tag{6}$$

As in classical Monte Carlo simulations, estimates of the thermodynamic averages can now be evaluated from configurations generated by the Metropolis algorithm, using $W(\vec{\mathbf{R}}_1,\ldots,\vec{\mathbf{R}}_M;\beta)$ defined in (6) in the transition matrix instead of the Boltzmann factor, $\exp[-\beta V(\vec{\mathbf{R}})]$. However, the number of particles in a path-integral quantum Monte Carlo simulation is larger than that of a classical simulation of the same size by a factor M. Clearly, a straightforward implementation of the classical Metropolis algorithm will be inefficient.

Takahashi and Imada[22] have proposed macroscopic and microscopic moves of the particles in the Metropolis sampling. The positions of all M particles on the chain are changed during the macroscopic move whereas only one of the $N\times M$ particles is moved during each microscopic move. The quantum-classical isomorphism suggests that the sampling may take advantage of the fact that the motion of the M particles on a chain are restrained by the harmonic potential. Following the work of Runge and Chester,[46] the Monte Carlo moves implemented in this work consist of changes in the normal-mode coordinates for the N polymer chains. By reexpressing the weight $W(\vec{\mathbf{R}}_1,\ldots,\vec{\mathbf{R}}_M;\beta)$ given in (6) in terms of the normal-mode coordinates, one can better appreciate the algorithm used in our work.

Three different types of attempted moves are used: (a) the center-of-mass coordinates $r_{\text{c.m.},j}$ of the polymer chains are displaced, (b) for each normal mode $\vec{k}$, the amplitudes, $\vec{q}^{(1)}_{k,j}$ and $\vec{q}^{(2)}_{k,j}$, of the modes associated with the polymer chains are changed sequentially, and (c) for each polymer chain, the high-frequency normal modes are grouped together so that their amplitudes are changed simultaneously in each attempted move; we refer to these as the multimode moves. The displacements of the normal-mode coordinates are adjusted so that the acceptances of all three kinds of moves generally range from 0.25 to 0.45. A Monte Carlo pass will consist of N of the center of mass moves for each polymer chain, N_q of indi-

vidual normal-mode moves for the N polymer chains, and followed by N_G of multimode moves for the N polymer chains. Each of the multimode moves has the same number of high-frequency modes. The algorithm guarantees that all modes for all polymer chains are moved in a Monte Carlo pass.

B. Model and simulations

Our simulations are performed at constant density ρ and temperature T with N particles confined within a cubic box. The side of the box L is chosen so that the box will enclose a lattice with periodic boundary conditions at density $\rho=N/L^3$. Ceperely, Chester, and Kalos[3,13,14] investigated the ground-state properties of particles interacting with the Yukawa pair interaction $v(r)$ of the form

$$v(r)=\epsilon\frac{\exp(-r/\sigma)}{r/\sigma} , \tag{7}$$

where ϵ has the dimension of energy and σ is the "screening" length. The reduced units in our work are defined by scaling energies by ϵ and lengths by σ. There is only one class of Yukawa systems and they interact via the reduced potential

$$v^*(r^*)=\frac{\exp(-r^*)}{r^*} , \tag{8}$$

where $r^*=r/\sigma$ is the reduced distance between particles. The system is parametrized by the reduced temperature $T^*=k_BT/\epsilon$ and the reduced density $\rho^*=\rho\sigma^3$. The quantum nature of the system is described by the de Boer parameter $\Lambda^*=\hbar^2/m\epsilon\sigma^2$, which can be regarded as a relative measure of the kinetic energy of the zero-point motion to the potential energy. All physical quantities will be expressed in reduced units and the asterisks are dropped in the text; that is, ρ is reduced density, T is reduced temperature, $v(r)$ is the reduced pair interaction between particles at reduced distance r, and so forth.

Using the algorithm outlined in Sec. II A, we have performed quantum Monte Carlo simulations for the truncated and shifted Yukawa potential given by

$$v(r)=\begin{cases}\exp\dfrac{(-r)}{r}-v(r_c) & \text{for } r\le r_c\\ 0 \quad \text{otherwise} , & \end{cases} \tag{9}$$

where r_c is the radius of truncation for the potential and is taken to be half the side of the box. The initial configuration has all M particles of each polymer chain at the same point and the N polymer chains are on the lattice sites. For the body-centered cubic lattice, we have studied systems with $N=54$ and 128. For the face-centered cubic lattice, depending on the density, systems with $N=108$, 256, 500, and 846 have been studied. However, the root-mean-square displacements from these simulations suggested that there are significant size dependence; namely the results depend strongly on the radius of cutoff r_c for the Yukawa potential. This is particularly true in the high-density systems. We resolved the difficulty of the significant dependence on r_c by defining the potential energy of the system as the sum of interactions between the particles and all their periodic images. This approach is essential in one-component plasma systems. However, since the Yukawa potential decays more rapidly than the Coulomb potential, our summation of the potential for the image particles is performed only for those in the 26 boxes surrounding the cubic system; images in the more distant boxes give an insignificant contribution. We refer to this as the extended Yukawa potential. The pair interaction between two particles at distance r is given by

$$v(r)=\sum_{\vec{\mathcal{N}}}\frac{\exp(-|\vec{r}-\vec{\mathcal{N}}L|)}{|\vec{r}-\vec{\mathcal{N}}L|} . \tag{10}$$

The sum is over the set of integers $\vec{\mathcal{N}}=(i,j,k)$ with $\{i,j,k\}\in\{-1,0,1\}$. The total potential energy V of the N-particle system also includes the interactions of the particles with their own images in the neighboring boxes but not with themselves, that is,

$$V(\vec{\mathbf{R}})=\sum_{i=1}^{N-1}\sum_{j=i+1}^{N}v(r_{ij})+\sum_{i=1}^{N}\sum_{\vec{\mathcal{N}}(\neq 0)}v(|\vec{\mathcal{N}}L|) . \tag{11}$$

The second term in (11) only contributes to the total potential energy. It remains unchanged throughout the Metropolis algorithm for the attempted moves and thus is ignored in the calculation of the changes in potential energy for generated configurations.

Using this extended potential, we have performed extensive quantum simulations at finite temperatures using the primitive algorithm to explore the phase diagram of the extended Yukawa system. The results presented in Sec. III are for simulations starting from the face-centered cubic lattice with $N=108$ particles at densities varying from 0.05 to 3.0. For $\Lambda^*=0.004$ and 0.005, simulations are performed along three isotherms: $T=0.004$, 0.006, and 0.008. The melting densities of the classical extended Yukawa systems at these temperatures lie in the range of 0.05 to 3.0. At $T=0.002$, runs were done also at $\Lambda^*=0.01$. The zero-temperature simulations suggest that there is no ground-state solid for the Yukawa bosons at $\Lambda^*=0.01$.[13] Since the Boltzmann particles have the same ground state as the bosons, these results suggest an interesting question: does the solid phase exist at any temperature? The number of time slices M used is chosen empirically and depends on the density, temperature and de Boer parameter; we have used $M=10$, 20, and 30. The simulation is started with the same initial configuration as that for the truncated and shifted Yukawa potential discussed earlier—a face-centered cubic lattice with M particles at each of the N lattice points. Subsequent configurations are generated with the Metropolis algorithm by performing the normal-mode moves. The Monte Carlo runs are monitored through the evolution of the potential energy U, the kinetic energy K, and the pressure P. These are given to $O((\beta/M)^2)$ (Refs. 22 and 36) by

$$U=\left\langle\frac{1}{M}\sum_{l=1}^{M}V(\vec{\mathbf{R}}_l)\right\rangle , \tag{12}$$

$$K=\left\langle\tfrac{3}{2}MNT-\frac{MT^2}{2\Lambda^*}\sum_{l=1}^{M}(\vec{\mathbf{R}}_l-\vec{\mathbf{R}}_{l+1})^2\right\rangle , \tag{13}$$

and

$$P=\rho TM-\frac{\rho T}{3}\left\langle\frac{MT}{N\Lambda^*}\sum_{l=1}^{M}(\vec{R}_{l+1}-\vec{R}_l)^2+\frac{1}{MNT}\sum_{l=1}^{M}\sum_{i=1}^{N-1}\sum_{j=i+1}^{N}\sum_{\vec{\mathcal{N}}}(\vec{r}_{i,l}-\vec{r}_{j,l}+\vec{\mathcal{N}}L)\cdot\frac{\partial v(|\vec{r}_{i,l}-\vec{r}_{j,l}+\vec{\mathcal{N}}L|)}{\partial(\vec{r}_{i,l}-\vec{r}_{j,l}+\vec{\mathcal{N}}L)}\right\rangle . \quad (14)$$

The angular brackets $\langle\cdots\rangle$ denote ensemble averages weighted by $W(\vec{R}_1,\ldots,\vec{R}_M;\beta)$ with respect to the $3N\times M$ coordinates in the box.

We did not attempt to locate, using free-energy calculations, the exact melting transitions of the various Yukawa systems we have studied. Before performing the involved calculations of free energies, the results from our simulations suggest that exchange effects are to be included in the model. The goal of this work is to demonstrate that for the soft-core systems, a high-density fluid phase exists. In the literature,[39] several empirical melting "laws" have been used to describe melting in classical systems. The most common ones are the Lindemann melting criterion in the solid and the static structure factor of fluids at freezing. The Lindemann ratio is the ratio of the root-mean-square displacement of the particles to the nearest-neighbor distance, and in a solid, it increases with temperature. The Lindemann criterion says that a solid melts at the temperature for which the Lindemann ratio reaches a critical value. At the freezing transition, the first peak of the static structure factor of most classical fluids has a value of 2.85. These one-phase criteria have yielded reasonable agreement between the melting properties obtained from experiments and computer simulations. Though we do not expect the quantum systems to have the same quantitative behavior, the melting "laws" are useful guidelines. To determine whether the system is a stable fluid, we use the following criteria.

1. Root-mean-square displacement, $\langle u_d^2\rangle^{1/2}$

In a solid, particles have low diffusivity and they are essentially bounded to the lattice sites. The particles in a solid are described in terms of motions about their lattice sites and we thus expect $\langle u_d^2\rangle^{1/2}$ to be bounded. However, in a fluid there is no well-defined lattice and the particles diffuse freely. We expect $\langle u_d^2\rangle^{1/2}$ in an infinite system to increase indefinitely. In our simulations, the motions of the particles are reflected in the root-mean-square displacement of the particles from their initial positions in a Monte Carlo run. With the quantum partition function approximated by (5), the root-mean-square displacement is given by

$$\langle u_d^2\rangle^{1/2}=\left[\frac{1}{NM}\left\langle\sum_{j=1}^{N}\sum_{l=1}^{M}|\vec{r}_j(l)-\vec{r}_{0,j}-\vec{\delta}_{\text{c.m.}}|^2\right\rangle\right]^{1/2}, \quad (15)$$

where $\vec{r}_{0,j}$ is the lattice site where all M particles of the jth polymer chain are initially located in the Monte Carlo run, and $\vec{\delta}_{\text{c.m.}}$ is the displacement of the center of mass of the configuration from the center of mass of the initial lattice.

To take into account the periodic boundary conditions, the center of mass of the configuration is defined to be that of the positions of the particles or their images which are nearest to their initial lattice sites. Thus any translation of the lattice, which may result from the periodic boundary conditions, will not be mistaken for random diffusion of the particles. For most classical systems, the Lindemann ratio of a solid at melting is roughly 0.17.[39] For the quantum solids at zero temperature, it is about 0.28.[13,14] Thus, if we start from a lattice and if the solid is the stable state at the density and temperature studied, the root-mean-square displacement will, after an initial increase, stay fairly constant with Monte Carlo passes at a value much less than the nearest-neighbor distance d of the lattice. However, if the fluid state is preferred, the lattice will collapse during the Monte Carlo run and the root-mean-square displacement will continue to increase, eventually reaching values larger than the nearest-neighbor distance of the initial lattice. The rate of increase of root-mean-square displacement with Monte Carlo passes, though a good guide to the stability of the solid phase, can only be reliably measured for long Monte Carlo runs. This is especially true if we encounter metastable states.

2. Static structure factor $S(\vec{K})$

The static structure factor $S(\vec{K})$ in the primitive approximation is

$$S(\vec{K})=\frac{1}{M}\sum_{l=1}^{M}S_l(\vec{K}), \quad (16)$$

where

$$S_l(\vec{K})=\left\langle\frac{1}{N}\sum_{j=1}^{N}\sum_{n=1}^{N}\exp[i\vec{K}\cdot(\vec{r}_{j,l}-\vec{r}_{n,l})]\right\rangle . \quad (17)$$

The sum in (17) is over all pairs of particles with the same time index l. Equation (17) looks like the structure factor of the particles with time index l, however the ensemble average is still weighted by $W(\vec{R}_1,\ldots,\vec{R}_M;\beta)$. The amplitude of the structure factor at the reciprocal-lattice vector reflects the periodicity of the underlying lattice. For the perfect lattice with N lattice points, the structure factor $S(\vec{K})$ at any reciprocal-lattice vector is clearly N. Its amplitude in a fluid is much lower because there is no periodicity in the system. From experiments and classical computer simulations, the first peak in a fluid phase has a value between 1 and 2, and the subsequent peaks are lower. We expect the peak heights of the static structure factor of the quantum solid to be much larger than those in the fluid phase. We calculate their values at several reciprocal lattice vectors to differentiate between the solid and fluid phases.

III. RESULTS OF SIMULATIONS

We have performed quantum Monte Carlo simulations at finite temperatures for Yukawa systems with de Boer

parameters $\Lambda^*=0.004$, 0.005, and 0.01. No exchange effects are included in this work: that is, the particles are distinguishable and obey Boltzmann statistics. These simulations are all carried out with the extended Yukawa potential, which has been defined in Sec. II B. The constant temperature and constant density simulations are performed along three isotherms: $T=0.004$, 0.006, and 0.008. (For $\Lambda^*=0.01$, simulations are also performed along $T=0.002$.) For each temperature T, we study the stability of the ordered solid phase at densities varying from 0.05 to 3.0. Using the melting criteria discussed in Sec. II B, which depend on the root-mean-square displacement of particles and the values of the structure factor at the first few reciprocal-lattice vectors, we have estimated the approximate boundaries between the fluid and solid phases. We will first present the results which lead to the schematic phase diagram and then will discuss the details of the motions of the particles.

A. Phase diagram of the quantum Yukawa systems

1. Root-mean-square displacement

Our constant-temperature and constant-density simulations are started from the face-centered cubic lattice of $N=108$ particles. The stability of the lattice has been determined from the change in the root-mean-square displacement of particles with the Monte Carlo passes during the run. The results from our quantum simulations will be grouped as follows.

(i) At de Boer parameter $\Lambda^*=0.004$ along the isotherm $T=0.004$ for densities $\rho=0.05$, 0.1, 0.3, 0.5, 1.0, 2.0, and 3.0.

(ii) At de Boer parameter $\Lambda^*=0.004$ along the isotherm $T=0.006$ for densities $\rho=0.1$, 0.3, 0.5, 1.0, 2.0, and 3.0.

(iii) At de Boer parameter $\Lambda^*=0.004$ along the isotherm $T=0.008$ for densities $\rho=0.3$, 0.5, 1.0, 2.0, and 3.0.

(iv) At de Boer parameter $\Lambda^*=0.005$ along the isotherm $T=0.004$ for densities $\rho=0.1$, 0.3, 0.5, 1.0, 2.0, and 3.0.

(v) At de Boer parameter $\Lambda^*=0.005$ along the isotherm $T=0.006$ for densities $\rho=0.1$, 0.3, 0.5, 0.75, 1.0, 2.0, and 3.0.

(vi) At de Boer parameter $\Lambda^*=0.005$ along the isotherm $T=0.008$ for densities $\rho=0.3$, 0.5, 1.0, 2.0, and 3.0.

(vii) At de Boer parameter $\Lambda^*=0.01$ along the isotherm $T=0.002$ for densities $\rho=0.3$ and 0.5.

(viii) At de Boer parameter $\Lambda^*=0.001$ along the isotherm $T=0.004$ for densities $\rho=0.1$, 0.3, 0.5, and 1.0.

Figures 1–8 show the Lindemann ratios obtained for these simulations. As discussed in Sec. II B, the change in the slope of the root-mean-square displacement with Monte Carlo passes is a crucial measure of the stability of the lattice. If the equilibrium state at the de Boer parameter, temperature and density (Λ^*,T,ρ) studied is a solid phase, the root-mean-square displacement of the system will eventually saturate at a constant value which is smaller than half the nearest-neighbor distance $d/2$ after an initial increase. Of course, the algorithm for the Metropolis sampling must guarantee that the system is ergodic for such a conclusion to be drawn.

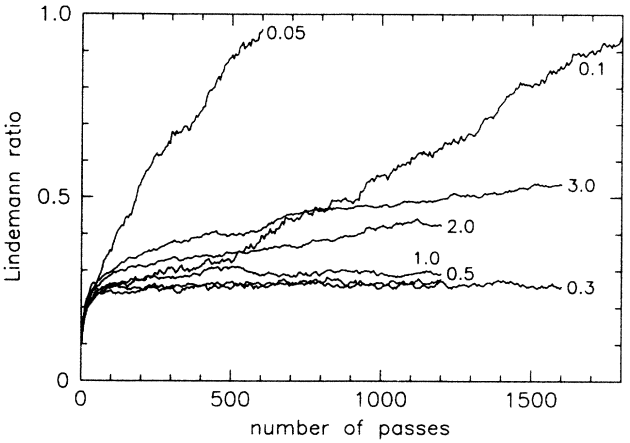

FIG. 1. Lindemann ratios of the quantum Yukawa systems at de Boer parameter $\Lambda^*=0.004$, the reduced temperature $T^*=0.004$, and reduced densities $\rho^*=3.0$, 2.0, 1.0, 0.5, 0.3, 0.1, and 0.05 as a function of the number of Monte Carlo passes. The Lindemann ratio is the ratio of the root-mean-square displacement of particles to the nearest-neighbor distance of the underlying face-centered cubic lattice. Each curve is labeled by the density of the run. The curves at $\rho^*=0.5$ and 0.3 almost overlap each other.

Figures 1–8 suggest that the quantum Yukawa solid is stable at $(\Lambda^*,T,\rho)=(0.004,0.004,0.3)$, $(0.004,0.004,0.5)$, $(0.004,0.004,1.0)$, $(0.004,0.006,0.5)$, $(0.005,0.004,0.3)$, and $(0.005,0.004,0.5)$. A long run was performed at $(\Lambda^*,T,\rho)=(0.005,0.004,0.5)$ to dispatch doubts on the

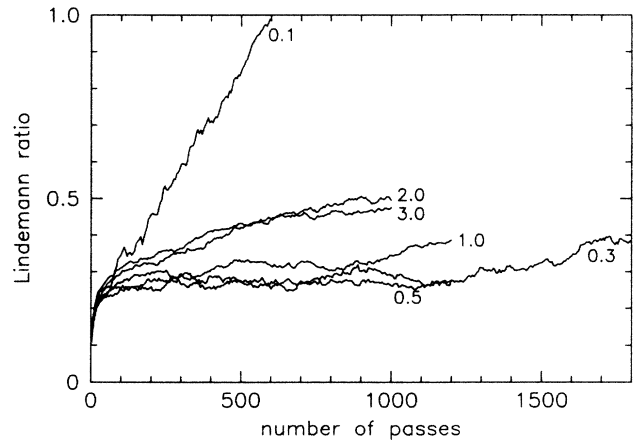

FIG. 2. Lindemann ratios of the quantum Yukawa system at de Boer parameter $\Lambda^*=0.004$, the reduced temperature $T^*=0.006$, and reduced densities $\rho^*=3.0$, 2.0, 1.0, 0.5, 0.3, and 0.1 as a function of the number of Monte Carlo passes. The Lindemann ratio is the ratio of the root-mean-square displacement of particles to the nearest-neighbor distance of the underlying face-centered cubic lattice. Each curve is labeled by the density of the run. The curve at $\rho^*=0.5$ ends at 1200 passes, merging with that at $\rho^*=0.3$.

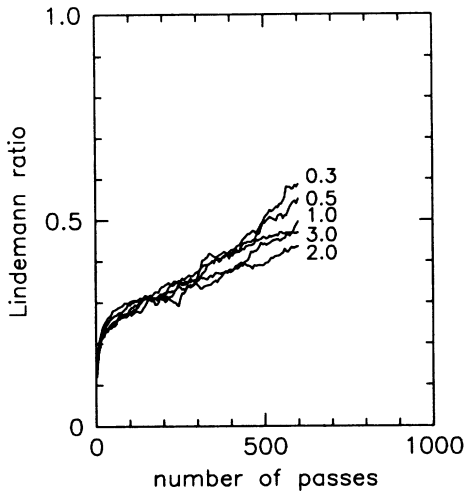

FIG. 3. Lindemann ratios of the quantum Yukawa system at de Boer parameter $\Lambda^*=0.004$, the reduced temperature $T^*=0.008$, and reduced densities $\rho^*=3.0$, 2.0, 1.0, 0.5, and 0.3 as a function of the number of Monte Carlo passes. The Lindemann ratio is the ratio of the root-mean-square displacement of particles to the nearest-neighbor distance of the underlying face-centered cubic lattice. Each curve is labeled by the density of the run. The curves are almost overlapping.

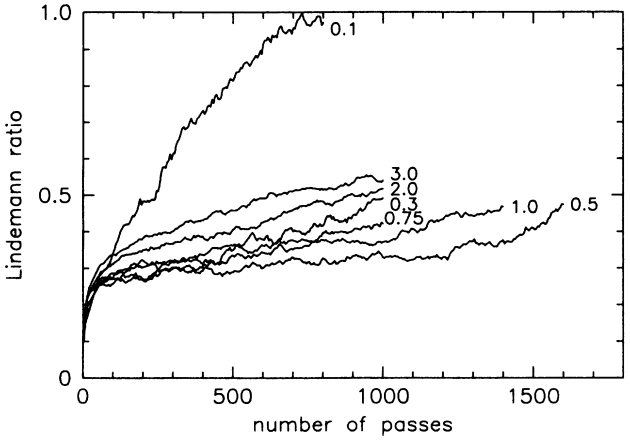

FIG. 5. Lindemann ratios of the quantum Yukawa system at de Boer parameter $\Lambda^*=0.005$, the reduced temperature $T^*=0.006$, and reduced densities $\rho^*=3.0$, 2.0, 1.0, 0.75, 0.5, 0.3, and 0.1 as a function of the number of Monte Carlo passes. The Lindemann ratio is the ratio of the root-mean-square displacement of particles to the nearest-neighbor distance of the underlying face-centered cubic lattice. Each curve is labeled by the density of the run.

stability of the lattice. At $T=0.008$, there is no solid found for densities ranging from 0.3 to 3.0 for both $\Lambda^*=0.004$ and $\Lambda^*=0.005$. At $\Lambda^*=0.01$ and $T=0.004$, the Yukawa solid is unstable for all densities between 0.1 and 1.0 studied. Similarly, at $T=0.002$, no solid is found at the densities $\rho=0.3$ and 0.5. The equilibrium state of the Yukawa systems at $(\Lambda^*,T)=(0.004,0.008)$, (0.005,0.008), (0.01, 0.002), and (0.01,0.004) is very likely a fluid phase at all densities. Sufficiently long runs are needed to differentiate a metastable system from a stable solid. This is particularly true for the runs at $(\Lambda^*,T,\rho)=(0.004,0.006,0.3)$ and (0.005,0.006,0.5). For example, during the Monte Carlo run for $(\Lambda^*,T,\rho)=(0.005,0.006,0.5)$, the root-mean-square displacement makes erratic jumps; it is only after approximately 1200 passes that one can identify the definite trend that the root-mean-square displacement is slowly increasing with Monte Carlo passes. An even longer run is needed for $(\Lambda^*,T,\rho)=(0.004,0.006,0.3)$; the breakdown of the lat-

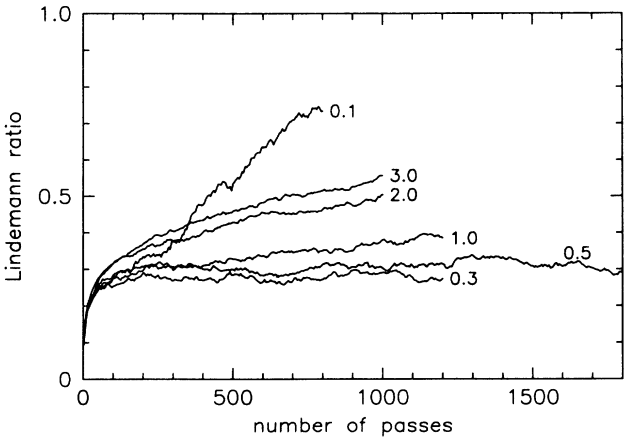

FIG. 4. Lindemann ratios of the quantum Yukawa system at de Boer parameter $\Lambda^*=0.005$, the reduced temperature $T^*=0.004$, and reduced densities $\rho^*=3.0$, 2.0, 1.0, 0.5, 0.3, and 0.1 as a function of the number of Monte Carlo passes. The Lindemann ratio is the ratio of the root-mean-square displacement of particles to the nearest-neighbor distance of the underlying face-centered cubic lattice. Each curve is labeled by the density of the run.

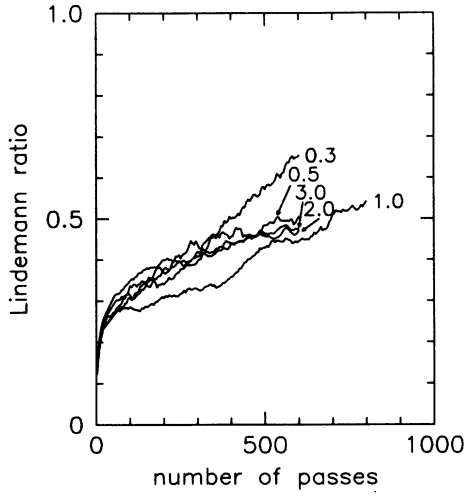

FIG. 6. Lindemann ratios of the quantum Yukawa system at de Boer parameter $\Lambda^*=0.005$, the reduced temperature $T^*=0.008$, and reduced densities $\rho^*=3.0$, 2.0, 1.0, 0.5, and 0.3 as a function of the number of Monte Carlo passes. The Lindemann ratio is the ratio of the root-mean-square displacement of particles to the nearest-neighbor distance of the underlying face-centered cubic lattice. Each curve is labeled by the density of the run. The curves at $\rho^*=3.0$ and 2.0 are very close to each other.

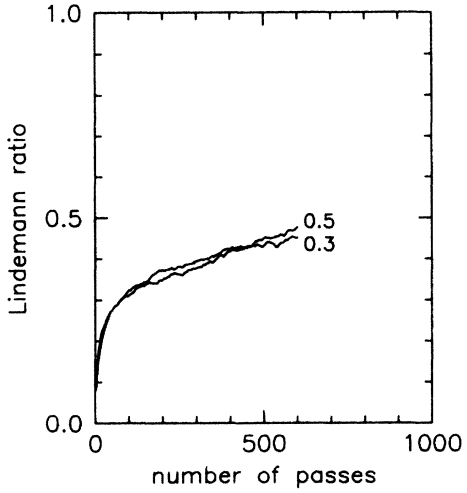

FIG. 7. Lindemann ratios of the quantum Yukawa system at de Boer parameter $\Lambda^*=0.01$, the reduced temperature $T^*=0.002$, and reduced densities $\rho^*=0.5$ and 0.3 as a function of the number of Monte Carlo passes. The Lindemann ratio is the ratio of the root-mean-square displacement of particles to the nearest-neighbor distance of the underlying face-centered cubic lattice. The curves are labeled by the densities of the runs.

tice is seen only after 1600 passes. For $(\Lambda^*,T,\rho)=(0.004,0.006,1.0)$, $(0.005,0.004,1.0)$, $(0.005,0.006,0.3)$, $(0.005,0.006,0.75)$, and $(0.005,0.006,1.0)$, the increase in root-mean-square displacement with Monte Carlo passes, though slow, is obvious. In some cases, at least 1000 passes are needed in the Monte Carlo run to firmly establish the gradual breakdown of the lattice. The slow increase in root-mean-square displacement for these metastable states is suggestive that these states are very close to the melting transitions; the metastable states need long Monte Carlo runs to each equilibrium.

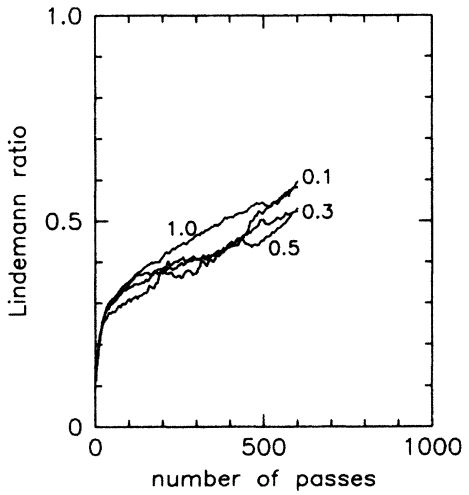

FIG. 8. Lindemann ratios of the quantum Yukawa system at de Boer parameter $\Lambda^*=0.01$, the reduced temperature $T^*=0.004$, and reduced densities $\rho^*=1.0$, 0.5, 0.3, and 0.1 as a function of the number of Monte Carlo passes. The Lindemann ratio is the ratio of the root-mean-square displacement of particles to the nearest-neighbor distance of the underlying face-centered cubic lattice. The curves are labeled by the densities of the runs and they almost overlap one another.

In the following section, the information from the structure factor calculations will establish more firmly our conclusions on the melting transitions of the quantum Yukawa systems discussed earlier. From the classical simulations of a range of inverse-power potentials,[47,48] it was found that the Lindemann ratio at melting is fairly independent of the details of the potential and is roughly 0.17. The ground-state study of the Yukawa boson found that the quantum solid melts when the Lindemann ratio is greater than 0.28.[13,14] For all of the solid phases identified in our quantum simulations, the Lindemann ratios do not exceed 0.3. We propose 0.3 to be an upper bound for the Lindemann ratio at melting for the extended quantum Yukawa systems at $T=0.004$ and 0.006.

2. *Structure factor*

We have evaluated the structure factor of the systems studied at several reciprocal-lattice vectors of the face-centered cubic lattice. As discussed in Sec. II B, we expect the amplitudes of the structure factor at the reciprocal-lattice vectors to show whether the system is in the solid or the disordered fluid phase. Table I lists the structure factors of the quantum systems at reciprocal lattice vectors (1,1,1), (1,1,−1), (1,−1,1), (−1,1,1), (2,0,0), (0,2,0), and (2,0,0). The reciprocal-lattice vectors are given in units of $\pi(2\rho)^{1/3}$. Each structure factor calculation is averaged over 40 configurations which span the last 200 passes in the Monte Carlo run. The results are grouped as in the preceding section.

The solid phases of the quantum Yukawa system identified from the structure factor calculations agree with the conclusions based on Lindemann ratios. The structure factors at [111] average more than 20 in the solid phases and are much smaller in the fluid phases, with values ranging mostly between 1 and 7. The structure factors at [200] follow a similar pattern: they average roughly 15 in the solids and 3 in the fluids. After the first 400 passes, the structure factor at the reciprocal lattice vector in the solid remains fairly constant with Monte Carlo passes, whereas in the fluid phases it decreases to values between 1 and 3. The particles in the solid are bound to their lattice sites and the periodicity of the lattice is preserved; this is reflected in the structure factor calculations. Although there are fluid phases with structure factors larger than 3 [in particular, we find that structure factors at $(\Lambda^*,T,\rho)=(0.004,0.006,1.0)$, $(0.005,0.004,1.0)$, and $(0.005,0.006,0.75)$ have values as high as 10], there is a definite trend for the structure factors to decrease during the Monte Carlo run. These fluid phases have not yet reached equilibrium. As we have pointed out, in some cases a long Monte Carlo run is needed to demonstrate the instability of the lattice. Even though our run for $(\Lambda^*,T,\rho)=(0.004,0.006,0.5)$ ended at 1200 passes with the same Lindemann ratio as $(\Lambda^*,T,\rho)=(0.004,0.006,0.3)$, which melted after 1600 passes, their structure factors are very different. At $(\Lambda^*,T,\rho)=(0.004,0.006,0.5)$, the structure factors at

[111] average roughly 25 and do not decrease during the run, whereas at $(\Lambda^*,T,\rho)=(0.004,0.006,0.3)$, the structure factors decrease slowly with the run. We are confident that the solid phase is stable at $(\Lambda^*,T,\rho)=(0.004,0.006,0.5)$ and it is not necessary to extend the run. When compared with results from classical simulations, which will be discussed in Sec. III A 3, the difference between the amplitudes of the structure factors in the solid and in the fluid phases is smaller for the quantum systems. The structure factor calculation is nevertheless a helpful tool for locating the melting transitions in the quantum systems.

3. *Comparison with classical phase diagram*

In addition to our quantum simulations, we have also performed classical simulations, using the standard Metropolis algorithm, for the extended Yukawa system.

TABLE I. Structure factors of the quantum Yukawa systems at de Boer parameter Λ^*, reduced temperature T^*, and reduced density ρ^*. The structure factors $S(\vec{K})$ are given at $\vec{K}$, the reciprocal-lattice vectors of the face-centered cubic lattice; $\vec{K}$ are in units of $\pi(2\rho^*)^{1/3}$.

			Structure factor at $\vec{K}$						
Λ^*	T^*	ρ^*	(111)	$(11\bar{1})$	$(1\bar{1}1)$	$(\bar{1}11)$	(200)	(020)	(002)
0.004	0.004	3.0	1.94	1.36	1.95	2.12	1.20	1.42	1.02
		2.0	4.55	4.15	3.56	6.08	2.24	2.17	1.61
		1.0	24.18	21.97	22.28	21.18	13.85	14.00	13.17
		0.5	25.58	28.91	25.99	28.66	18.36	17.51	17.85
		0.3	29.81	32.02	26.95	28.72	17.58	19.95	20.67
		0.1	1.35	0.88	1.58	1.54	1.22	0.95	1.31
		0.05	2.53	1.09	2.83	2.17	1.05	0.88	1.11
	0.006	3.0	2.38	3.85	2.63	3.46	1.47	1.06	1.56
		2.0	3.35	2.57	1.86	2.91	1.15	1.27	1.05
		1.0	9.60	11.72	7.52	10.41	4.43	5.37	4.01
		0.5	27.65	32.41	25.81	29.71	19.58	20.17	16.91
		0.3	10.70	6.06	10.19	4.38	3.45	5.25	3.77
		0.1	2.04	2.00	1.83	2.57	1.33	0.83	1.80
	0.008	3.0	4.82	2.21	2.42	2.52	1.45	1.08	1.33
		2.0	5.99	6.21	6.13	6.43	1.88	2.44	3.36
		1.0	4.24	4.33	4.54	4.43	2.33	1.58	1.45
		0.5	2.16	3.70	2.13	4.47	1.12	1.15	2.21
		0.3	1.69	2.66	6.94	2.33	2.26	0.89	0.89
0.005	0.004	3.0	1.98	1.75	1.80	2.03	1.10	1.42	1.21
		2.0	2.57	1.95	4.31	3.08	1.47	1.46	1.74
		1.0	10.28	8.48	8.02	8.18	4.68	4.09	4.88
		0.5	17.74	16.53	20.86	22.02	10.16	10.64	13.03
		0.3	25.22	24.96	25.13	23.97	14.66	15.60	15.92
		0.1	0.82	0.96	0.91	1.90	0.92	0.98	1.33
	0.006	3.0	1.52	1.78	1.60	2.26	1.21	1.09	1.35
		2.0	2.97	2.25	1.91	3.25	1.18	1.04	1.17
		1.0	3.04	2.98	3.97	2.61	1.15	1.53	1.69
		0.75	5.24	10.20	3.06	6.44	3.65	3.15	2.45
		0.5	6.79	5.81	5.74	5.96	2.03	4.06	2.56
		0.3	7.89	5.38	7.56	5.55	4.86	2.67	3.36
		0.1	2.27	1.68	1.32	2.07	1.13	0.98	0.95
	0.008	3.0	3.24	2.44	3.88	2.81	1.81	1.30	1.24
		2.0	2.76	5.36	4.56	4.44	1.75	2.05	1.96
		1.0	4.33	5.80	8.24	2.07	2.41	1.72	2.08
		0.5	6.84	3.30	1.45	1.62	1.66	1.30	1.19
		0.3	4.86	1.11	2.68	1.47	1.37	1.28	0.86
0.01	0.004	1.0	2.39	1.82	2.43	1.84	1.16	1.26	1.14
		0.5	2.75	4.02	3.14	4.22	2.24	1.45	1.75
		0.3	2.86	3.50	2.29	3.90	1.44	1.48	1.44
		0.1	2.92	3.29	1.42	5.55	1.40	2.06	1.17
	0.002	0.5	4.09	3.52	3.93	4.44	2.19	1.90	2.16
		0.3	5.15	3.93	5.63	3.86	2.74	2.21	2.45

In this section, we will compare our results from these simulations performed along the isotherms $T=0.004$, 0.006, and 0.008 with densities varying from 0.1 to 3.0 with those from the quantum simulations (the densities studied are $\rho=0.1$, 0.3, 0.5, 1.0, 2.0, and 3.0). As for the quantum simulations, our constant-temperature and constant-density classical simulations are started from a face-centered cubic lattice of $N=108$ particles enclosed in a box with periodic boundary conditions. From the discussion in Sec. II B, we see that the number of degrees of freedom in a quantum simulation is more than that of a classical simulation with the same number of particles by a factor of M, where M is the number of time slices used. In our case, this will be a factor of 10–30. Furthermore, the extended Yukawa pair potential is not truncated and we cannot take advantage of any neighborhood-table construct in calculating the potential energy. For our classical simulations, 3000 Monte Carlo passes are performed for most of the runs. In some cases, only 2000 Monte Carlo passes are needed to clearly establish whether the equilibrium phase is solid or fluid. Longer runs are needed for the systems close to the melting transition; the longest run requires 6500 passes. The melting transition is determined from the root-mean-square displacement of the particles, and from structure factors calculated at reciprocal-lattice vectors. The longer Monte Carlo runs for the classical simulations make it easier to locate the melting transitions.

The change of root-mean-square displacement of particles with Monte Carlo passes can be crudely estimated from the slope of the curve by performing linear regression on the "straight" line portion of the curve towards the end of the run. Table II lists the estimated average change of the root-mean-square displacement over 1000 passes. The entries which have negative slope also have negative coefficient of correlation. The root-mean-square displacement fluctuates about a constant in these cases. The changes of root-mean-square displacement of particles in the classical and quantum systems are similar. The rate of change in the fluid phase is faster than in the solid phase by at least a factor of 10, and for the same phase, are of the same order of magnitude in both systems. At $T=0.004$ and $T=0.006$, the classical Yukawa system is a stable solid for densities $\rho=0.3$ and larger. At $T=0.008$, the melting transition occurs between $\rho=0.5$ and $\rho=0.3$. The Lindemann ratio of these classical systems is not larger than 0.2, which is much smaller than its quantum value. Table III lists the structure factors calculated from the last configurations in the Monte Carlo runs. The heights of the first peaks of the structure factors in the classical solids average more than 40; this average height is at least twice as high as in the quantum systems. In the fluids, the structure factors only average about 5 at most. This striking difference between the structure factors of the solids and the fluids makes it easier to locate the melting transition in the classical systems. The fluid phases which can be identified from Table III, namely $(\rho,T)=(0.1,0.004)$, (0.1,0.006), (0.1,0.008), and (0.3, 0.008), support our conclusion drawn from the behavior of root-mean-square displacement. At each of the temperatures studied, only one melting transition is observed in our classical simulations. At temperatures of $T=0.008$ and lower, the high-density systems with $\rho=1.0$ or more are solids—there is no high-density classical fluid phases at these low temperatures. Pressure melting at finite temperatures in the soft-

TABLE II. Changes in root-mean-square displacement of particles, Δu_d, with Monte Carlo passes in classical and quantum Yukawa systems at de Boer parameter Λ^*, reduced temperature T^*, and reduced density ρ^*. Δu_d given, which is estimated by performing linear regression, is for 1000 passes and is given in units of reduced nearest-neighbor distance of the face-centered cubic lattice.

			Δu_d over 1000 passes		
			Quantum systems with de Boer parameter Λ^*		
T^*	ρ^*	Classical	0.004	0.005	0.01
0.004	3.0	0.000 38(160)	0.1025 (21)	0.1628 (36)	
	2.0	0.001 29(110)	0.1405 (35)	0.1122 (38)	
	1.0	−0.007 06(438)	0.002 46 (279)	0.1225 (54)	0.3522 (168)
	0.5	0.002 39(417)	0.006 76 (292)	0.001 51 (255)	0.4519 (317)
	0.3	0.000 25(180)	0.004 97 (145)	0.019 95 (542)	0.4103 (173)
	0.1	0.3981 (77)	0.5102 (51)	0.7061 (120)	0.7614 (211)
0.006	3.0	0.002 26(153)	0.091 02 (378)	0.1554 (54)	
	2.0	−0.003 16(219)	0.1686 (46)	0.2281 (52)	
	1.0	0.002 94(377)	0.2177 (50)	0.1860 (60)	
	0.5	0.000 24(253)	−0.015 02 (328)	0.2152 (82)	
	0.3	0.002 59(339)	0.2060 (62)	0.2417 (81)	
	0.1	0.3042 (144)	1.301 (27)	0.6712 (198)	
0.008	3.0	0.006 50(201)	0.3275 (79)	0.2162 (137)	
	2.0	−0.005 40(184)	0.2557 (93)	0.2272 (115)	
	1.0	0.006 41 (76)	0.5377 (96)	0.4007 (110)	
	0.5	0.005 81(831)	0.5485 (176)	0.2252 (261)	
	0.3	0.3400 (84)	0.7585 (133)	0.7982 (171)	
	0.1	0.2565 (98)			

TABLE III. Structure factors of the classical Yukawa systems at reduced temperature T^* and reduced density ρ^*. The structure factors $S(\vec{K})$ are given at $\vec{K}$, the reciprocal-lattice vectors of the face-centered cubic lattice; $\vec{K}$ are in units of $\pi(2\rho^*)^{1/3}$.

		Structure factor at $\vec{K}$						
T^*	ρ^*	(111)	$(11\bar{1})$	$(1\bar{1}1)$	$(\bar{1}11)$	(200)	(020)	(002)
0.004	3.0	98.69	98.07	100.77	100.79	97.11	95.27	98.51
	2.0	97.45	96.86	95.34	96.30	95.16	89.41	94.99
	1.0	95.19	97.59	96.12	95.69	94.32	91.74	91.38
	0.5	87.35	83.40	83.36	76.56	69.11	79.66	77.81
	0.3	75.65	79.73	84.62	78.73	77.68	71.17	68.85
	0.1	2.05	0.03	0.55	3.23	0.07	0.47	0.06
0.006	3.0	92.29	92.41	90.26	95.54	89.70	89.21	85.45
	2.0	95.36	95.21	94.76	93.78	89.99	90.84	91.37
	1.0	79.06	77.55	83.54	88.30	69.91	77.71	76.45
	0.5	68.43	80.82	61.71	76.55	58.09	69.38	60.21
	0.3	70.85	64.90	69.05	63.38	62.72	52.44	57.45
	0.1	0.16	3.16	6.42	3.71	1.97	0.34	0.48
0.008	3.0	91.83	91.22	89.74	90.60	83.30	88.19	85.82
	2.0	93.49	84.64	94.36	89.86	81.88	89.26	84.88
	1.0	64.85	73.74	70.61	73.64	67.03	56.87	60.63
	0.5	57.97	47.05	58.76	49.54	40.80	45.71	38.74
	0.3	1.66	2.84	3.30	4.87	0.15	1.01	0.49
	0.1	3.51	0.37	3.60	0.04	0.92	0.21	0.57

core Yukawa system is observed only if quantum effects are included.

In addition to the runs discussed above, the melting temperatures for the classical extended Yukawa systems are determined more precisely from other runs at densities between 0.1 and 3.0. The schematic phase diagram is given in Fig. 9 together with those of the quantum Yukawa systems at de Boer parameter $\Lambda^*=0.004$ and 0.005. For each of the quantum systems, the coexistence curve forms a loop bounded by the density axis. As the quantum nature of the Yukawa system becomes more important, the loop shrinks and the solid phase spans a smaller region in the phase diagram. The difference between the two melting densities at a fixed temperature decreases with increasing de Boer parameter. The zero-temperature phase diagrams of the Yukawa boson and fermion determined by Ceperley, Chester, and Kalos (see Fig. 4 in Refs. 13 and 14) indicate that there is no ground-state Yukawa solid at any density when Λ^* is larger than a critical value Λ_c^*. For the bosons, Λ_c^* is estimated at 0.0057 from exact calculations and is at 0.0094 from variational studies. Variational fermion calculations suggest Λ_c^* to be at 0.013. The zero-temperature studies are for a model system different from ours—we do not consider exchange effects and our potential energy also includes the interaction of the image particles in the neighboring boxes. Since the soft-core nature of the Yukawa potential is important in pressure melting, we expect the ground-state phase diagram of the extended Yukawa system to be qualitatively similar; of course, exchange effects cannot be excluded at absolute zero. None of the systems studied at $\Lambda^*=0.01$, even at the lower temperature of $T=0.002$, has a stable solid phase. It is possible that there is no Yukawa solid with $\Lambda^*=0.01$ at any density and any temperature. Thus when the de Boer parameter becomes larger than some critical value, the solid region in the phase diagram may disappear entirely. To prove the above statement, in particular to exclude the existence of a closed solid-region in the phase diagram entirely closed by the fluid phase—a "bubble"—will require more extensive simulations.

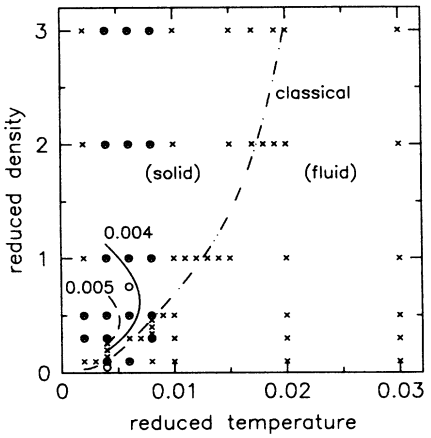

FIG. 9. Phase diagrams of the classical Yukawa system and the quantum Yukawa systems at de Boer parameters $\Lambda^*=0.004$ and 0.005. The solid-fluid coexistence curves are schematic and are located by the instability of the lattice. They are given by the dashed-dotted line for the classical system, the solid line for the quantum system at $\Lambda^*=0.004$, and the dashed line for that at $\Lambda^*=0.005$. For each system, the solid region is to the left of the coexistence curve and bounded by the density axis. Simulations are performed at the densities and temperatures marked by $\times$ for the classical systems and by $\circ$ for the quantum systems.

B. Properties of the Yukawa quantum fluids and solids

1. Motion of the particles

In Sec. III A 1, we have discussed the significance of the root-mean-square displacement of the particles. We have used this to determine the stability of the initial lattice in our Monte Carlo runs. Successive configurations generated by the Metropolis algorithm in a Monte Carlo run form a random walk in the configuration space. Though the motion of particles along a Monte Carlo chain does not bear any direct relation to their diffusivity in real time, it does reflect whether or not particles in a system are localized in space. In the primitive approximation, a "chain" of M particles is associated with an "original particle" in the system. Following the quantum-classical isomorphism of (5), the chain can also be pictured as a wave-packet identified with the "particle" and its spread may be thought of as a measure of the extent of the zero-point motion of the "particle." We thus use interchangeably the notion of paths and chains to describe the quantum systems.

In addition to the root-mean-square displacement of particles given in (15), we define the mean path size and root-mean-square displacement of the center of mass of paths, or chains, to describe the motion of particles in these quantum systems. As in all previous definitions, periodic boundary conditions are taken into consideration. The center of mass of the jth path $\vec{r}_{\text{c.m.},j}$ is defined to be

$$\vec{r}_{\text{c.m.},j}=\vec{r}_{j,1}+\frac{1}{M}\sum_{l=2}^{M}(\vec{r}_{j,l}-\vec{r}_{j,1}-\vec{\mathcal{N}}_{j,l}L)\ , \tag{18}$$

and the mean path size λ_p is then given by

$$\lambda_P=\left[\frac{1}{NM}\sum_{j=1}^{N}\sum_{l=1}^{M}|\vec{r}_{j,l}-\vec{r}_{\text{c.m.},j}-\vec{\mathcal{N}}_{j,l}|^2\right]^{1/2}, \tag{19}$$

where $\vec{\mathcal{N}}_{j,l}$ in both definitions is chosen so that the sum is over the difference between $\vec{r}_{j,1}$ and the nearest image of $\vec{r}_{j,l}$. Only paths near to the surface of the box will be affected by the periodic boundary conditions. The root-mean-square displacement of the centers of mass of paths is defined as

$$\langle u^2_{\text{c.m.}}\rangle^{1/2}=\left[\frac{1}{N}\left\langle\sum_{j=1}^{N}|\vec{r}_{\text{c.m.},j}-\vec{r}_{o,j}-\vec{\delta}_{\text{c.m.}}|^2\right\rangle\right]^{1/2}. \tag{20}$$

Any translation of the lattice as a whole is accounted for in $\vec{\delta}_{\text{c.m.}}$. Table IV lists the root-mean-square displacement of particles, the mean path size and the root-mean-square displacement of the centers of mass of paths. These are calculated from the last configurations in the Monte Carlo runs and are given in units of the nearest-neighbor distance d. Table IV also lists the fractions of particles and paths which are displaced from their original lattice sites by more than half the nearest-neighbor distance. These particles and paths have left their original cell in the starting configuration. Table V lists the rates of increase of the root-mean-square displacement of both the particles and the center of mass of paths, and the rate of increase of the mean path size with Monte Carlo passes at various densities with $(\Lambda^*,T)=(0.004,0.004)$. These are obtained from linear regression typically on the results of 40 analyses from the last 200 passes of the runs. We have performed longer runs at $(\Lambda^*,T)=(0.004,0.004)$ and densities $\rho=3.0$ (the high-density fluid), 0.3 (the solid phase), and 0.1 (the low-density fluid) and hope to understand more about the motion of particles in the quantum systems. Several general trends in the mobility of the quantum fluids can be drawn from the results shown in Figs. 1–8, and Tables II, IV, and V. Note that the lengths of the Monte Carlo runs varies from system to system.

The quantum system is parametrized by the de Boer parameter, density and temperature, (Λ^*,ρ,T). The mean path size for each of the systems studied remains fairly constant after the system has reached equilibrium. The number of passes required clearly depends on the magnitude of the "spring constant" in the effective potential in (5). The mean path size of the low-density system is much smaller than the nearest-neighbor distance. None of the paths extends to the nearest-neighbor cell and there are no overlaps between the paths. At any density, the mean path size becomes larger with increasing de Boer parameter and decreasing temperature. This behavior resembles that of the thermal de Broglie wavelength. At any (Λ^*,T), though the mean path size decreases only slightly with increasing density, the nearest neighbors get closer and eventually the paths overlap. When this happens, one must seriously reconsider the validity of ignoring exchange effects in our model. We believe that pressure melting results from the presence of a soft core in the Yukawa potential. In the classical theory of freezing, the reduction in free volume in high-density systems is important since freezing is regarded as a packing phenomenon. In the quantum Yukawa system, we believe that the high-density solid is unstable because the particles can tunnel through the local potential barriers and are not localized. When exchange becomes important, it will only enhance the instability of the lattice. The details of the phase diagram will be changed, but the solid will still undergo the melting transition to the high-density fluid. The above speculation can only be confirmed by detailed simulations which take into account exchange effects.

The root-mean-square displacement of the centers of mass of the paths is less than that of the particles and this difference increases with the density of the system. Both displacements, however, evolve along the Monte Carlo runs with the same rate in all the systems we have studied. In the solid phase, they both eventually level to some constant, whereas in the fluid phase, they both increase along the Monte Carlo run at some finite rate. At any (Λ^*,T), the high-density fluid is less diffusive than the low-density fluid. We also find that in the high-density fluid, the fraction of paths with their centers of mass displaced more than half the nearest-neighbor distance is much smaller than that of the particles. From these results, we see that the diffusivity of the quantum fluid is attributable to both the very extended nature of the

"paths" associated with the particles and with the motion of these paths. It is important to note that the mean path size in the high-density fluid remains fairly constant throughout the run and that the increase in the root-mean-square displacement of the particles results mainly from the paths diffusing away from the lattice. The particles do not remain localized and the lattice is unstable: the high-density solid melts.

2. *Pair distribution function*

The pair distribution function $g(\vec{r})$ is the probability of finding two particles at the separation $\vec{r}$. In simulations,

TABLE IV. The root-mean-square displacements of particles, of the center of mass of paths, and the mean path size of the quantum Yukawa systems at de Boer parameter $\Lambda^*=0.004$, reduced temperature T^*, and reduced density ρ^*. The root-mean-square displacements of particles $\langle u_d^2 \rangle^{1/2}$, of the center of mass of paths $\langle u_{\text{c.m.}}^2 \rangle^{1/2}$, and the mean path size λ_P are given in units of the reduced nearest-neighbor distance of the face-centered cubic lattice $d^*=2^{1/6}/\rho^{*1/3}$, where ρ^* is the reduced density of the system. f_{msd}, $f_{\text{c.m.}}$, and f_{sz}, respectively, give the fractions of particles with mean displacements, center-of-mass displacements, and path size larger than $d^*/2$.

Λ^*	T^*	ρ^*	$\langle u_d^2 \rangle^{1/2}$	f_{msd}	$\langle u_{\text{c.m.}}^2 \rangle^{1/2}$	$f_{\text{c.m.}}$	λ_P	f_{sz}
0.004	0.004	3.0	0.53	0.46	0.37	0.20	0.38	0.028
		2.0	0.42	0.24	0.28	0.0	0.32	0.0
		1.0	0.29	0.04	0.15	0.0	0.25	0.0
		0.5	0.28	0.02	0.16	0.0	0.23	0.0
		0.3	0.26	0.02	0.16	0.0	0.20	0.0
		0.1	0.94	0.87	0.93	0.86	0.16	0.0
		0.05	0.96	0.83	0.95	0.82	0.15	0.0
	0.006	3.0	0.47	0.35	0.35	0.10	0.32	0.0
		2.0	0.50	0.37	0.39	0.15	0.30	0.0
		1.0	0.39	0.17	0.30	0.06	0.24	0.0
		0.5	0.28	0.02	0.18	0.0	0.21	0.0
		0.3	0.38	0.17	0.33	0.12	0.19	0.0
		0.1	1.08	0.88	1.07	0.89	0.15	0.0
	0.008	3.0	0.47	0.35	0.37	0.10	0.29	0.0
		2.0	0.44	0.27	0.34	0.09	0.27	0.0
		1.0	0.50	0.39	0.44	0.31	0.22	0.0
		0.5	0.55	0.46	0.52	0.37	0.19	0.0
		0.3	0.59	0.55	0.56	0.52	0.18	0.0
0.005	0.004	3.0	0.56	0.50	0.35	0.11	0.43	0.139
		2.0	0.50	0.39	0.32	0.05	0.39	0.046
		1.0	0.39	0.16	0.25	0.02	0.29	0.0
		0.5	0.31	0.06	0.16	0.0	0.24	0.0
		0.3	0.27	0.03	0.16	0.0	0.22	0.0
		0.1	0.73	0.69	0.71	0.64	0.19	0.0
	0.006	3.0	0.54	0.44	0.38	0.19	0.39	0.046
		2.0	0.52	0.42	0.39	0.13	0.34	0.009
		1.0	0.47	0.31	0.38	0.16	0.27	0.0
		0.75	0.42	0.20	0.33	0.08	0.26	0.0
		0.5	0.47	0.34	0.41	0.20	0.24	0.0
		0.3	0.49	0.29	0.45	0.22	0.20	0.0
		0.1	0.97	0.83	0.96	0.82	0.16	0.0
	0.008	3.0	0.48	0.32	0.33	0.10	0.34	0.018
		2.0	0.47	0.32	0.36	0.16	0.31	0.0
		1.0	0.41	0.21	0.32	0.07	0.25	0.0
		0.5	0.54	0.46	0.46	0.30	0.21	0.0
		0.3	0.51	0.37	0.63	0.56	0.19	0.0
0.01	0.004	1.0	0.58	0.51	0.34	0.09	0.47	0.296
		0.5	0.53	0.42	0.36	0.19	0.39	0.074
		0.3	0.52	0.40	0.41	0.21	0.33	0.009
		0.1	0.60	0.48	0.54	0.36	0.24	0.0
	0.002	0.5	0.48	0.35	0.21	0.0	0.43	0.065
		0.3	0.45	0.28	0.23	0.0	0.39	0.074

TABLE V. Changes in root-mean-square displacement of particles Δu_d, of the center of mass of paths $\Delta u_{\text{c.m.}}$, and the mean path size Δu_λ over Monte Carlo passes of the quantum Yukawa system at de Boer parameter $\Lambda^*=0.004$, reduced temperature $T^*=0.004$ and reduced density ρ^*. The changes given, which are estimated by performing linear regression, are for 1000 passes and are in units of reduced nearest-neighbor distance of the face-centered cubic lattice d^*. Δf_{msd} and $\Delta f_{\text{c.m.}}$ are, respectively, the corresponding changes in the fraction of particles with $\langle u_d^2\rangle^{1/2}$ and $\langle u_{\text{c.m.}}^2\rangle^{1/2}$ larger than $d^*/2$.

ρ^*	Δu_d	Δf_{msd}	$\Delta u_{\text{c.m.}}$	$\Delta f_{\text{c.m.}}$	Δu_λ
3.0	0.103 (2)	0.183 (5)	0.127 (2)	0.262 (9)	0.026 (2)
2.0	0.141 (4)	0.039 (33)	0.088 (18)	−0.001 (26)	−0.047 (9)
1.0	0.003 (3)	0.053 (13)	0.050 (14)	0.0	0.029 (7)
0.5	0.007 (3)	0.007 (10)	0.049 (15)	0.0	−0.001 (7)
0.3	0.005 (1)	−0.007 (2)	−0.017 (5)	0.0	0.016 (2)
0.1	0.510 (5)	0.490 (8)	0.525 (5)	0.551 (11)	−0.002 (1)
0.05	1.046 (14)	0.521 (56)	0.999 (40)	0.560 (72)	0.020 (7)

one usually calculates the angular-averaged pair distribution function $g(r)$. In the primitive approximation, $g(r)\,dr$ is essentially the probability of finding two particles with the same time index separated by distance ranging between r and $r+dr$. It is calculated from

$$g(r)=\left\langle \frac{2L^3}{MN(N-1)\mathcal{V}_{\text{shell}}(r,r+dr)} \sum_{l=1}^{M} N_p(r,r+dr;l) \right\rangle , \tag{21}$$

where $\mathcal{V}_{\text{shell}}(r,r+dr)$ is the volume of the shell from radius r to $r+dr$ which is enclosed inside the cube of side L, and $N_p(r,r+dr;l)$ is the total number of distinct pairs of particles of time index l whose distance of separation is between r and $r+dr$.

The angular-averaged pair distribution function of a classical solid with long-range positional order has well-defined peaks at distances determined by the underlying lattice. Though these peaks broaden and lower with increasing temperature, the pair distribution function of a solid is distinctly different from that of a fluid and is a valuable tool for locating melting transitions in classical systems. Figure 10 shows the pair distribution functions of the classical Yukawa fluid at $(T,\rho)=(0.004,0.1)$ and, of the solid at $(T,\rho)=(0.004,0.3)$ and $(0.004,0.5)$. The radial distance is given in units of the nearest-neighbor distance d. The positions of the four peaks in $g(r)$ of the solid phase correspond well with the distances to the first four neighbors on the face-centered cubic lattice: d, $1.41d$, $1.73d$, and $2d$. The first peak in the fluid is much lower than in the solid, while the second peak, which is much smaller, has been washed out. The melting density of the classical solid at $T=0.004$ is $\rho=0.012$. Even very close to the melting transition at $\rho=0.013$, the first peak in $g(r)$ is 1.23 times higher than that of the fluid at $\rho=0.012$, although the small second peak near $r=1.41d$ (see Fig. 10) has disappeared. The situation for quantum solids and fluids is strikingly different. There are no significant differences between the pair distribution functions of the quantum solids and fluids studied in our simulations. The height of the first peak in the solids is no more than 1.8, and is typically about 1.65. In the

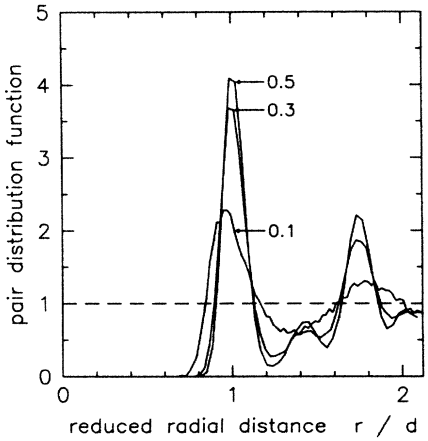

FIG. 10. Pair distribution functions $g(r/d)$ of the classical Yukawa systems at the reduced temperature $T^*=0.004$ and the reduced density ρ^*: solids at $\rho^*=0.5$ and 0.3, and the fluid at $\rho^*=0.1$. The distance r is scaled by the nearest-neighbor distance d of the underlying face-centered cubic lattice. The maximum radial distance given, $2.12d$, is half the side of the cube of the face-centered cubic lattice with $N=108$ particles. The dashed straight line is at $g(r)=1$.

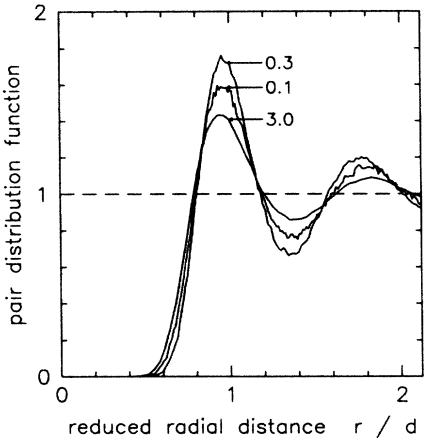

FIG. 11. Pair distribution functions $g(r/d)$ of the quantum Yukawa systems with de Boer parameter $\Lambda^*=0.004$ at the reduced temperature $T^*=0.004$ and the reduced density ρ^*: high-density fluid at $\rho^*=3.0$, solid at $\rho^*=0.3$, and low-density fluid at $\rho^*=0.1$. The distance r is scaled by the nearest-neighbor distance d of the underlying face-centered cubic lattice. The maximum radial distance given, $2.12d$, is half the side of the cube of the face-centered cubic lattice with $N=108$ particles. The dashed straight line is at $g(r)=1$.

fluids, it varies between 1.4 and 1.6. We might, however, expect that the differences in $g(r)$ for the quantum fluid and solid phases will be more pronounced at large separation r. The computational time needed to study pressure melting in bigger extended Yukawa systems is unrealistically long using our current algorithm and the available computers.

Though the pair distribution function cannot provide a melting criterium for the quantum systems, it provides some interesting information. Figure 11 gives the pair distribution functions at $(\Lambda^*,T)=(0.004,0.004)$ and $\rho=3.0$, 0.3, and 0.1. Despite the big difference in the root-mean-square displacement of the particles of the solid at $\rho=0.3$ and the fluids at $\rho=0.1$ and 3.0, their pair distribution functions are very similar. From Table IV, we note that at $(\Lambda^*,T)=(0.004,0.004)$, both the root-mean-square displacement of particles and the fraction of particles of the high-density fluid at $\rho=3.0$ which have left their original cell is twice as large as in the low-density fluid at $\rho=0.1$. Surprisingly the pair distribution

TABLE VI. The reduced total energy E^*, kinetic energy K^*, and pressure P^* of the quantum Yukawa systems at de Boer parameter Λ^*, reduced temperature T^*, and reduced density ρ^*. f_E is the fraction of total energy which is contributed from tail correction; similarly, f_P is that for pressure. f_K is the ratio of the quantum kinetic energy to its classical value $1.5T^*$.

Λ^*	T^*	ρ^*	E^*	P^*	K^*	f_K	f_E	f_P
0.004	0.004	3.0	20.65	70.48	0.0789	13.2	18.5	28.0
		2.0	13.00	29.89	0.0737	12.3	14.3	22.9
		1.0	5.83	6.78	0.0539	9.0	8.1	14.6
		0.5	2.60	1.53	0.0427	7.1	3.8	7.7
		0.3	1.41	0.509	0.0281	4.7	1.9	4.2
		0.1	0.365	0.0473	0.0177	2.9	0.24	0.63
		0.05	0.147	0.0101	0.0129	2.1	0.04	0.12
	0.006	3.0	20.68	70.54	0.0948	10.5	18.5	28.0
		2.0	13.00	29.89	0.0718	8.0	14.3	22.9
		1.0	5.84	6.79	0.0611	6.8	8.1	14.6
		0.5	2.59	1.53	0.0395	4.4	3.8	7.7
		0.3	1.42	0.51	0.0321	3.6	1.9	4.2
		0.1	0.370	0.0476	0.0200	2.2	0.24	0.63
	0.008	3.0	20.70	70.57	0.1079	9.0	18.5	28.0
		2.0	13.01	29.91	0.0820	6.8	14.3	22.9
		1.0	5.85	6.79	0.0629	5.2	8.1	14.6
		0.5	2.60	1.53	0.0418	3.5	3.8	7.7
		0.3	1.42	0.511	0.0344	2.9	1.9	4.2
0.005	0.004	3.0	20.65	70.49	0.0808	13.5	18.5	28.0
		2.0	13.01	29.89	0.0731	12.2	14.3	22.9
		1.0	5.83	6.78	0.0537	9.0	8.1	14.6
		0.5	2.61	1.53	0.0446	7.4	3.8	7.7
		0.3	1.43	0.512	0.0372	6.2	1.9	4.1
		0.1	0.368	0.0475	0.0192	3.2	0.24	0.63
	0.006	3.0	20.69	70.55	0.0981	10.9	18.5	28.0
		2.0	13.01	29.90	0.0753	8.4	14.3	22.9
		1.0	5.85	6.79	0.0632	7.0	8.1	14.6
		0.75	4.19	3.66	0.0578	6.4	6.1	11.5
		0.5	2.62	1.53	0.0495	5.5	3.8	7.7
		0.3	1.42	0.511	0.0337	3.8	1.9	4.2
		0.1	0.373	0.0478	0.0217	2.4	0.24	0.63
	0.008	3.0	20.71	70.60	0.1104	9.2	18.5	28.0
		2.0	13.03	29.92	0.0854	7.1	14.3	22.9
		1.0	5.86	6.80	0.0694	5.8	8.1	14.6
		0.5	2.61	1.53	0.0442	3.7	3.8	7.7
		0.3	1.43	0.512	0.0375	3.1	1.9	4.1
0.01	0.004	1.0	5.88	6.80	0.0653	10.9	8.1	14.6
		0.5	2.62	1.54	0.0468	7.8	3.8	7.7
		0.3	1.45	0.515	0.0416	6.9	1.8	4.1
		0.1	0.377	0.0481	0.0221	3.7	0.24	0.62
	0.002	0.5	2.61	1.53	0.0404	13.5	3.8	7.7
		0.3	1.44	0.513	0.0363	12.1	1.9	4.1

TABLE VII. The reduced total energy E^*, kinetic energy K^*, and pressure P^* of the classical Yukawa systems at reduced temperature T^* and reduced density ρ^*. f_E an f_P are, respectively, the fractions of total energy and pressure which are contributed from tail corrections.

T^*	ρ^*	E^*	P^*	f_E	f_P
0.004	3.0	20.45	70.13	18.7	28.2
	2.0	12.83	29.69	14.4	23.1
	1.0	5.72	6.72	8.2	14.7
	0.5	2.52	1.51	3.9	7.8
	0.3	1.36	0.500	1.9	4.2
	0.1	0.341	0.0457	0.25	0.65
0.006	3.0	20.45	70.14	18.7	28.2
	2.0	12.83	29.70	14.4	23.1
	1.0	5.73	6.72	8.2	14.7
	0.5	2.53	1.51	3.9	7.8
	0.3	1.37	0.501	1.9	4.2
	0.1	0.348	0.0461	0.25	0.65
0.008	3.0	20.46	70.16	18.7	28.2
	2.0	12.84	29.71	14.4	23.1
	1.0	5.73	6.73	8.2	14.7
	0.5	2.53	1.51	3.8	7.8
	0.3	1.38	0.503	1.9	4.2
	0.1	0.353	0.0464	0.25	0.64

functions of these fluids suggest that the high-density fluid is less correlated than the low-density fluid. The mean path size in the high-density fluid is large and comparable to the average distance between particles (see Sec. III B 1), and so the exact locations of particles are less correlated.

3. *Thermodynamic properties—energy and pressure*

The total potential energy and pressure estimated from our simulations include the interactions of the image particles in the neighboring boxes. The Yukawa pair potential is effectively truncated at different distances for different densities. We calculate the tail corrections for the potential energy U and pressure P using the expressions[39]

$$\frac{U}{N}=\tfrac{1}{2}\rho\int d\vec{r}\,g(r)v(r)\ , \tag{22}$$

and

$$\frac{\beta P}{\rho}=1-\tfrac{1}{6}\beta\rho\int d\vec{r}\,g(r)r\frac{dv(r)}{dr}\ . \tag{23}$$

The integration is over all space outside the extended box of length $1.5L$ (L is the side of the periodic cube enclosing the particles). The first order approximation is to take the pair distribution function $g(r)$ outside the box to be unity for both the solid and fluid phases.

The total energy per particle and pressure, including the tail corrections, from our quantum simulations are listed in Table VI, and those for the classical systems are given in Table VII. The quantum partition function in (5) is exact only in the limit of M approaching infinity, and so the thermodynamic quantity estimated from ensemble averages weighted by the weight $W(\vec{R}_1,\ldots,\vec{R}_M;\beta)$ is M dependent. An accurate estimate for any thermodynamic quantity can only be obtained from extrapolation via a large M. Though we have not performed such extrapolations in our simulations, M has been chosen to be sufficiently big so that errors in the thermodynamic quantities are expected to be fairly small. Any comparison to be made with the values listed in the table should keep this in mind. The kinetic energy of the quantum systems studied is at least a factor of 2 more than the classical kinetic energy, which is $1.5T$. This factor increases with decreasing temperature, increasing de Boer parameter, and increasing density as the quantum nature of the system becomes more important.

IV. SUMMARY AND DISCUSSIONS

The phase diagrams of the quantum Yukawa systems with an extended potential at de Boer parameters $\Lambda^*=0.004$, 0.005, and 0.01 have been explored using the path-integral Monte Carlo method. In our work, the systems obey Boltzmann statistics. The melting transition is located by the stability of the lattice during the Monte Carlo runs. The phase diagrams of the quantum systems at $\Lambda^*=0.004$ and $\Lambda^*=0.005$ and of the classical extended Yukawa system are shown schematically in Fig. 9. Both quantum systems demonstrate pressure melting. Along the low-temperature isotherm, say $T=0.004$, the low-density fluid freezes into a solid as the density is increased. When the density is increased further, the solid phase melts at the upper transition into a high-density fluid. The coexistence curve, as drawn, does not violate the Clausius-Clapeyron relation if we assume that the entropies of both the high- and low-density fluids are larger than of the solids at coexistence. At $\Lambda^*=0.01$, the solid phase is unstable at all the temperatures and densities

studied: $(T,\rho)=(0.004,1.0)$, $(0.004,0.5)$, $(0.004,0.3)$, $(0.004,0.1)$, $(0.002,0.5)$, $(0.002,0.3)$. From Fig. 9, we note that the region where the solid is stable becomes smaller with increasing de Boer parameter. Using the face that, for both bosons and fermions, there is no Yukawa solid at zero temperature at any density when Λ^* is sufficiently large,[13,14] we suggest that there may be no solid at any density and any temperature for the extended Yukawa system at de Boer parameter $\Lambda^*=0.01$. If the de Boer parameter is greater than some critical value, the only phase for the extended Yukawa system at all densities and all temperatures is the fluid phase. Even though the particles are less diffusive in the high-density fluids, their positions are less correlated than in the low-density fluids, as shown by the pair distribution functions.

The exact thermodynamic phase transitions between the solid and fluid phases can be located via free-energy calculations. Various methods have been introduced to calculate free energies which cannot be computed directly from the standard Metropolis sampling algorithm.[49,50] The most straightforward method is to perform a suitable thermodynamic integration, basically either of any energy with respect to temprature or of pressure with respect to density.[49] For the Yukawa systems, we would need to compute free energies for the solids, the low-density fluids and also the high-density fluids. Since the free energy at zero temperature, which is just the energy, can be obtained from Green's function Monte Carlo simulations, in principle, one can perform the energy integration from zero temperature to obtain free energies for all three phases. However, the energies estimated from simulations, in particular at very low temperatures, have to be very accurate to yield an acceptable polynomial fit to the thermal energy $[E_{\rm th}(T)=E(T)-E(T=0)]$ for the thermodynamic integration. One should really perform the extrapolation to large M to get accurate estimates of energies from the path-integral Monte Carlo simulations. Furthermore, simulations at very low temperatures will require a large number of time slices which will be very costly. [For example, in the quantum simulation at $(\Lambda^*,T,\rho)=(0.005,0.004,3.0)$ with $M=30$ and $N=108$ we can only perform about 40 Monte Carlo passes per central-processing-unit hour on a Cray Research X-MP/48 computer.] The free energy of the solid phase could be obtained by using the method of Frenkel and Ladd.[51] This, however, will involve simulations in the presence of interacting harmonic potential. Any other method to obtain acceptable estimates for free energies of the three phases in the Yukawa systems will require more extensive simulations.

The results from our simulations indicate that exchange effects, which have been ignored from our model, are very likely to be significant, especially in the high-density fluids at the temperatures studied. It will thus be inappropriate to perform the costly calculations for free energies to locate the coexistence curve accurately. Our quantum simulations on the extended Yukawa systems using the path-integral Monte Carlo method have still successfully demonstrated pressure melting, which is consequence of the soft core of the Yukawa pair potential.

ACKNOWLEDGMENTS

We would like to thank Karl Runge for his helpful discussions and the quantum Monte Carlo codes which we adapted for our work. The quantum simulations were performed on the Cray Research X-MP/48 computer at the National Center for Supercomputing Applications (Urbana, IL) and the classical simulations were run on the Floating Point Systems FPS-264 array processors at the Cornell National Supercomputer Facility (Ithaca, NY). We would like to acknowledge the support from the National Science Foundation under Contract No. DMR-85-13300.

*Present address: Theoretical Physics Institute, School of Physics and Astronomy, University of Minnesota, Minneapolis, Minnesota 55455.

[1]Daniel Schiff, Nat. Phys. Sci. **243**, 130 (1973).
[2]J. P. Hansen, B. Jancovici, and Daniel Schiff, Phys. Rev. Lett. **29**, 991 (1972).
[3]D. M. Ceperley and G. V. Chester, Phys. Rev. D **13**, 3208 (1976).
[4]Jean Pierre Hansen and Redha Mazighi, Phys. Rev. A **18**, 1282 (1978).
[5]R. Mochkovitch and J. P. Hansen, Phys. Lett. **73A**, 35 (1979).
[6]J. P. Hansen, R. Mazighi, and P. Viellefosse, Phys. Lett. **81A**, 215 (1981).
[7]Hikaru Kawamura, Prog. Theor. Phys. **66**, 772 (1981).
[8]D. A. Kirzhnits, Zh. Eksp. Teor. Fiz. **38**, 503 (1960) [Sov. Phys.—JETP **11**, 365 (1960)].
[9]Khiaru Kawamura and Kuniyoshi Ebina, Phys. Lett. **103A**, 273 (1984).
[10]H. R. Glyde, G. H. Keech, R. Mazighi, and J. P. Hansen, Phys. Lett. **58A**, 226 (1976).
[11]D. M. Ceperley, Phys. Rev. B **18**, 3126 (1978).
[12]D. M. Ceperley and B. J. Alder, Phys. Rev. Lett. **45**, 566 (1980).
[13]D. Ceperley, G. V. Chester, and M. H. Kalos, Phys. Rev. B **17**, 1070 (1978).
[14]D. Ceperley, G. V. Chester, and M. H. Kalos, Phys. Rev. B **16**, 3081 (1977).
[15]Hikaru Kawamura, Prog. Theor. Phys. **64**, 419 (1980).
[16]Hikaru Kawamura, Prog. Theor. Phys. **66**, 421 (1981).
[17]P. P. Ewald, Ann. Phys. **64**, 253 (1921).
[18]Mario P. Tosi, in *Solid State Physics*, edited by F. Seitz and D. Turnbull (Academic, New York, 1964) Vol. 16, see Appendix A.
[19]J. A. Barker, J. Chem. Phys. **70**, 2914 (1979).
[20]David Chandler and Peter G. Wolynes, J. Chem. Phys. **74**, 4078 (1981).
[21]M. F. Herman, E. J. Bruskin, and B. J. Berne, J. Chem. Phys. **78**, 5150 (1982).
[22]Minoru Takahashi and Masatoshi Imada, J. Phys. Soc. Jpn. **53**, 963 (1984).

[23]E. L. Pollock and D. M. Ceperley, Phys. Rev. B **30**, 2555 (1984).

[24]R. P. Feynman and A. R. Hibbs, *Quantum Mechanics and Path Integrals* (McGraw-Hill, New York, 1965).

[25]L. S. Schulman, *Techniques and Applications of Path Integration* (Wiley, New York, 1981).

[26]*NATO Workshop on Monte Carlo Methods in Quantum Problems,* edited by Malvin H. Kalos (Reidel, Dordrecht, The Netherlands, 1984), Vol. 125C. Several articles are on path-integral quantum integral methods.

[27]Proceedings of the Conference on Frontiers of Quantum Monte Carlo, Los Alamos, New Mexico, 1986, edited by James E. Gubernatis [J. Stat. Phys. **43**, Nos. 5/6 (1986)].

[28]D. M. Ceperley, in Proceedings of the International School of Physics, "Enrico Fermi", Course XCVII, Varenna, 1985, edited by G. Ciccotti and W. G. Hoover (North-Holland, New York, 1986).

[29]D. M. Ceperley and E. L. Pollock, Phys. Rev. Lett. **56**, 351 (1986).

[30]Farid F. Abraham and Jeremy Q. Broughton, Phys. Rev. Lett. **59**, 64 (1987).

[31]Masatoshi Imada, J. Phys. Soc. Jpn. **53**, 2861 (1984).

[32]Masatoshi Imada and Minoru Takahashi, J. Phys. Soc. Jpn. **53**, 3770 (1984).

[33]Minoru Takahashi and Masatoshi Imada, J. Phys. Soc. Jpn. **53**, 3871 (1984).

[34]M. Parrinello and A. Rahman, J. Chem. Phys. **80**, 860 (1984).

[35]Bart De Raedt, Michiel Sprik, and Michael L. Klein, J Chem. Phys. **80**, 5719 (1984).

[36]Minoru Takahashi and Masatoshi Imada, J. Phys. Soc. Jpn. **53**, 3765 (1984).

[37]M. Creutz and B. Freedman, Ann. Phys. (N.Y.) **132**, 427 (1981).

[38]R. P. Feynman, *Statistical Mechanics* (Benjamin, Reading, 1982).

[39]J. P. Hansen and I. R. McDonald, *Theory of Simple Liquids,* 1st ed. (Academic, London, 1976); *Theory of Simple Liquids,* 2nd ed. (Academic, London, 1986).

[40]N. Metropolis, A. W. Rosenbluth, M. N. Rosenbluth, A. H. Teller, and E. Teller, J. Chem. Phys. **21**, 1087 (1953).

[41]David Ceperley and Berni Alder, Science **231**, 555 (1986).

[42]Gianni Jacucci, in *NATO Workshop on Monte Carlo Methods in Quantum Problems,* edited by Malvin H. Kalos (Reidel, Dordrecht, The Netherlands, 1984), Vol. 125C.

[43]D. Thirumalai, Randall W. Hall, and B. J. Berne, J. Chem. Phys. **81**, 2523 (1984).

[44]Hans De Raedt and Bart De Raedt, Phys. Rev. A **28**, 3575 (1983).

[45]Kenneth S. Schweizer, Richard M. Stratt, David Chandler, and Peter G. Wolynes, J. Chem. Phys. **75**, 1347 (1981).

[46]Karl Runge and G. V. Chester, Phys. Rev. B (to be published).

[47]William G. Hoover, Steven G. Gray, and Keith W. Johnson, J. Chem. Phys. **55**, 1128 (1971).

[48]Jean Pierre Hansen and Daniel Schiff, Mol. Phys. **25**, 1281 (1973).

[49]J. P. Valleau and G. M. Torrie, *Statistical Mechanics A, Modern Theoretical Chemistry,* edited by B. J. Berne (Plenum, New York, 1977), Vol. 5.

[50]M. P. Allen and D. J. Tildesley, *Computer Simulation of Liquids* (Oxford University Press, New York, 1987).

[51]D. Frenkel and A. Ladd, J. Chem. Phys. **81**, 3188 (1984).